Further orbital-free kinetic-energy functionals for *ab initio* molecular dynamics

Michael Foley and Paul A. Madden
Physical Chemistry Laboratory, Oxford University, South Parks Road, Oxford OX1 3QZ, United Kingdom
(Received 26 October 1995)

A recently introduced scheme for *ab initio* molecular-dynamics with an orbital-free density functional [Phys. Rev. B **49**, 5220 (1994)] is extended so that the kinetic-energy functional guarantees correct results at third order of perturbation theory. The new density functional gives improved accuracy, yielding good agreement with well-converged Kohn-Sham results for many properties of metals such as aluminum. This molecular-dynamics scheme retains many of the advantages of the old: it is very fast, exhibits close to linear scaling with system size, and may be readily ''conditioned'' to maximize the molecular-dynamics time step.

I. INTRODUCTION

In recent work the possibility has been demonstrated[1,2] of basing an accurate *ab initio* molecular-dynamics (MD) method on an ''orbital-free'' formulation of density-functional theory (DFT). The obvious advantage of this formulation over the normal Car-Parrinello method, [3–5] where a Kohn-Sham (K-S),[6] orbital-based representation of DFT is used, is that the electronic part of the calculation scales linearly with system size (i.e., it is an ''order N'' method). Several other, less obvious advantages have also been uncovered. The algorithm may be straightforwardly ''conditioned''[1] so that the MD time step is optimized and *independent of system size*. This means that the method is order N in practice as well as in principle. The method is most advantageous for metals, where it has proven possible[2] to construct an orbital-free representation with the accuracy of Kohn-Sham theory. For metals the conditioned algorithm gives adiabatic dynamics, unlike the Kohn-Sham–based method. [7,8] Furthermore, since wave functions are not used, Brillouin-zone sampling is not required to calculate metallic properties accurately. The power of the method has been demonstrated in calculations on metallic liquids[9] and on point defect formation free-energies.[10,11]

The principle problem in finding an accurate orbital-free density functional is to represent the kinetic-energy functional of a noninteracting electron gas.[12,13] It is worth noting that crude approximations are useless: the virial theorem shows that the kinetic energy of the electrons is comparable to their total energy. The K-S representation is, in principle, exact, but in the plane-wave-based methods of most interest in simulation,[5] it gives technical problems for the simplest metals, where extensive Brillouin-zone sampling is required to represent the Fermi sphere. For these systems it has been shown that orbital-free functionals that incorporate several exact limiting forms provide extreme accuracy. The uniform gas limit is represented by the Thomas-Fermi (T-F) functional,

$$T = T_{\text{T-F}} = c_k \int d\mathbf{r} \rho^{5/3}(\mathbf{r}), \tag{1.1}$$

(where ρ is the electron density) while the strong potentials limit (strictly, the large $s = |\nabla\rho|/\rho^{4/3}$ limit) is given by the von Weizsäcker (vW) functional,[14,13]

$$T_{\text{vW}} = \frac{1}{2}\int d\mathbf{r} \rho^{1/2}\nabla^2\rho^{1/2} = \frac{1}{8}\int d\mathbf{r} |\nabla\rho|^2/\rho. \tag{1.2}$$

These terms are modified to guarantee that they give the correct response behavior for perturbations about the uniform gas limit, as suggested by Perrot[15] and Wang and Teter.[16] The response functionals of the noninteracting electron system are known exactly[17] and they may be embedded into the kinetic-energy functional, as originally indicated by Hohenberg and Kohn.[18] A full discussion of the nature of these functionals and the different ways in which the embedding may be attempted is given in Ref. 2. Finally, we note that Alavi and co-workers[19] have proposed an orbital-free functional on a quite different basis that is more general than our approach but is less convenient computationally.

In the work done to date,[1,2] the correct *linear* response was included. For sodium, with a local pseudopotential[20] known from K-S calculations to give good agreement with experiment, this linear response functional was shown to reproduce accurately a wide variety of static and dynamic experimental data, including the vacancy formation energy of the solid, inelastic neutron scattering data on the liquid, etc. Results for aluminium were also discussed:[2] this is known to be a more difficult case, since effective pair potentials, based on linear response theory, do not correctly reproduce experimental properties such as the vacancy formation energy.[21] For aluminium a comparison with fully converged K-S calculations,[22,23] with a particular local pseudopotential,[24] on a variety of crystal structures and solid-state properties was made and also with experiment.[25,26] It was shown that the orbital-free code gave accurately the energies of crystals with high coordination numbers (fcc, bcc, etc.) and good results for their phonon dispersion curves. However, for more open structures (diamond, vacancy lattice, etc.) errors in the energy of order 0.2 eV per atom were found. An analysis of the role of different orders of perturbation theory was undertaken, following an idea of Gillan.[23] It was shown that while the beyond-linear response characteristics of the functional agreed with those of K-S calculations when evaluated for the high coordination structures, for the open structures errors at the third order of perturbation theory became apparent (i.e., at the level of second-order response of the density). It was

concluded that an extended functional, into which the correct *second-order* response function was embedded, might make an accurate represention of materials such as aluminum possible.

This paper describes further work to develop such a functional for use in *ab initio* MD and to evaluate the functional both for its accuracy, in representing materials such as aluminium, and for its computational performance with respect to other methods. A valuable background to this development was provided by the paper of Wang and Teter,[16] who have already proposed a second-order response functional and shown how it may be rendered into a computationally tractable form. This functional was used only in the context of energy calculations; forces were not discussed. We show that the scheme results in an order N MD method, which may be conditioned in the same way as with the linear response functional.

II. DEVELOPMENT OF THE FUNCTIONAL

In the work to date,[1,2] correct *linear* response has been embedded and the resulting functionals are of the form

$$T_\alpha[\rho]=T_{\text{T-F}}[\rho]+T_{\text{vW}}[\rho]+\int_\Omega d\mathbf{r}\int d\mathbf{r}'\,\Delta\rho^{(\alpha)} \times(\mathbf{r})K_\alpha(\mathbf{r}-\mathbf{r}')\Delta\rho^{(\alpha)}(\mathbf{r}'), \tag{2.1}$$

where $\Delta\rho^{(x)}(\mathbf{r})=\rho^x(\mathbf{r})-\rho_0^x$, with ρ_0 the uniform density, and Ω is the volume of the periodically repeated simulation cell. The response kernel K_α is most readily expressed in reciprocal space,

$$K_\alpha(g)=-\frac{1/\chi_0-1/\chi_{\text{vW}}-1/\chi_{\text{T-F}}}{2\alpha^2\Omega\rho_0^{2(\alpha-1)}}. \tag{2.2}$$

χ_0 is the linear response function of the noninteracting homogeneous electron gas, i.e., the Lindhard function,[27] and $\chi_{\text{T-F}}=3\rho_0/k_F^2$ (k_F is the Fermi wave vector) and $\chi_{\text{vW}}=4\rho_0/g^2$ are the response functions associated with the Thomas-Fermi and von Weizsäcker kinetic-energy functionals.[28]

The basic strategy, as clearly seen in the $\alpha=1$ functional,[15] is to add a quadratic term in the density fluctuations [which contains the linear response (Refs. 18 and 28)] to $T_{\text{T-F}}+T_{\text{vW}}$ *minus* their quadratic parts. The limiting behaviors are therefore built in. Away from these limits, the functional can be criticized on two grounds. Firstly, the beyond-linear response is not correct. This is particularly true at low g where it is known that the correct nonlinear behavior is given by the gradient-corrected Thomas-Fermi result $T_{\text{T-F}}[\rho_0]+1/9T_{\text{vW}}$.[12] On the other hand, at high g, $T_{\text{T-F}}+T_{\text{vW}}$ should give the nonlinear response quite well.[13] Secondly, adding the different terms in this way means that they continue to contribute in domains where they are inapplicable. For example, T_{vW} gives the *exact* kinetic energy for a one-electron ground state[13] but, if Eq. (2.1) is used for the hydrogen atom, the other two terms will not disappear, and they give spurious contributions to the kinetic energy. Ideally the limiting forms would be combined in a more subtle way so that this did not happen.

To some extent, these objections may be met by different choices of α, as can be seen by looking at the reciprocal space expressions for the general functional:

$$T_\alpha[\rho]=\Omega\sum_{\mathbf{g}}\left\{\frac{3k_F^2}{10\rho_0^{2/3}}\rho_{\mathbf{g}}^{(5/6)}\rho_{-\mathbf{g}}^{(5/6)}+\frac{1}{2}\rho_{\mathbf{g}}^{(1/2)}g^2\rho_{-\mathbf{g}}^{(1/2)} -\frac{1}{2\alpha^2\rho_0^{2(\alpha-1)}}\rho_{\mathbf{g}}^{(\alpha)}\frac{1}{\chi_0(g)}\rho_{-\mathbf{g}}^{(\alpha)} -\frac{k_F^2}{6\alpha^2\rho_0^{2\alpha-1}}\rho_{\mathbf{g}}^{(\alpha)}\rho_{-\mathbf{g}}^{(\alpha)} -\frac{1}{8\alpha^2\rho_0^{2\alpha-1}}\rho_{\mathbf{g}}^{(\alpha)}g^2\rho_{-\mathbf{g}}^{(\alpha)}\right\}, \tag{2.3}$$

where, for instance, $\rho_{\mathbf{g}}^{(1/2)}$ denotes the $\mathbf{g}$th Fourier component of $\rho^{(1/2)}(\mathbf{r})$.

For the choice of $\alpha=5/6$, due to Wang and Teter,[16] the first and fourth terms can be combined — $T_{\text{T-F}}$ could be incorporated within the double integral. In this sense, the linear response term grows naturally out of the Thomas-Fermi functional. Perrot has pointed out[15] a potentially important consequence of this choice for the way this functional behaves in the limit of low density (i.e., the ''atomic'' limit where the degree of ionization of a collection of atoms is low). The double integral in Eq. (2.1) will diverge as $\rho_0\to 0$ if $\alpha>5/6$, leading to an infinite atomic kinetic energy, and if $\alpha<5/6$ the double integral will disappear, so that the linear response correction will be lost.

Similarly, $T_{1/2}$ has a von Weiszäcker-like double integral. In this case the second and fifth terms exactly cancel, implying that T_{vW} is already contained within the χ_0^{-1} term. Furthermore, for the $g\to 0$ components of the sum, $\chi_0^{-1}(g)\to -1/3\rho_0(k_F^2+g^2/12)$, canceling the fourth term and leaving the $\mathbf{g}$th Fourier component of $1/9T_{\text{vW}}$, that is, the gradient correction to $T_{\text{T-F}}$. Thus, $T_{1/2}$ correctly yields the gradient-corrected Thomas-Fermi result $T_{\text{T-F}}[\rho_0]+1/9T_{\text{vW}}$ in the low-$\mathbf{g}$ limit.

As indicated previously, the beyond-linear response characteristics of these functionals are already important for aluminimum. Our strategy in this work is to generalize the functionals to embed *second*-order response exactly and then we hope that the beyond second-order behavior is sufficiently well captured by some way of combining the limiting forms.

A. Introducing the correct quadratic response

To quadratic order in the Fourier components of the perturbing potential $V(\mathbf{g})$, the induced charge density $\Delta\rho_{\mathbf{g}}$ in a noninteracting electron gas is given by

$$\Delta\rho_{\mathbf{g}}=\chi_0(g)V(\mathbf{g}) +\frac{1}{\pi^2k_F}\sum_{\mathbf{g}_1}\sum_{\mathbf{g}_2}\delta_{\mathbf{g}_1+\mathbf{g}_2-\mathbf{g}}I(g_1,g_2,g)V(\mathbf{g}_1)V(\mathbf{g}_2), \tag{2.4}$$

where $\delta_{\mathbf{x}}$ is the Kronecker delta. A complete and accurate derivation of $I(g_1,g_2,g)$, appears in Refs. 29 and 30. If $g_1+g_2=g_3$, then I is given by

$$I(g_1,g_2,g_3)=-\frac{\pi^2k_F^2}{6g_1g_2g_3}\{g_1\chi_0(g_1)+g_2\chi_0(g_2)-g_3\chi_0(g_3)\}. \quad (2.5)$$

Otherwise it is given by

$$I(g_1,g_2,g_3)=U(\mathbf{g}_1,\mathbf{g}_2)+U(\mathbf{g}_1,\mathbf{g}_3)+U(\mathbf{g}_2,\mathbf{g}_3), \quad (2.6)$$

and $\mathbf{g}_1+\mathbf{g}_2+\mathbf{g}_3=0$. If θ is the angle between $\mathbf{g}_1$ and $\mathbf{g}_2$ and $q_i=g_i/k_F$, then for $q_3^2-4\sin^2\theta\geqslant 0$,

$$U(\mathbf{g}_1,\mathbf{g}_2)=\frac{1}{4q_1q_2\sin^2\theta}\left\{(q_1\cos\theta+q_2)\ln\left|\frac{2+q_1}{2-q_1}\right|+(q_2\cos\theta+q_1)\ln\left|\frac{2+q_2}{2-q_2}\right|+\sqrt{q_3^2-4\sin^2\theta}\times\ln\left|\frac{4\cos\theta+q_1q_2-2\sqrt{q_3^2-4\sin^2\theta}}{4\cos\theta+q_1q_2+2\sqrt{q_3^2-4\sin^2\theta}}\right|\right\}, \quad (2.7)$$

and for $q_3^2-4\sin^2\theta\leqslant 0$,

$$U(\mathbf{g}_1,\mathbf{g}_2)=\frac{1}{4q_1q_2\sin^2\theta}\left\{(q_1\cos\theta+q_2)\ln\left|\frac{2+q_1}{2-q_1}\right|+(q_2\cos\theta+q_1)\ln\left|\frac{2+q_2}{2-q_2}\right|-2\sqrt{4\sin^2\theta-q_3^2}\left[h(q_1q_2+4\cos\theta)\pi+\tan^{-1}\left(\frac{-2\sqrt{4\sin^2\theta-q_3^2}}{q_1q_2+4\cos\theta}\right)-\frac{\pi}{3}\right]\right\}, \quad (2.8)$$

where

$$h(x)=\begin{cases}1 & \text{when } x\geqslant 0\\ 0 & \text{when } x<0.\end{cases} \quad (2.9)$$

[The expression differs from that given in Ref. 16 in the appearance of factors of $\pi/3$ in Eq. (2.8). These arise from a proper account of poles that occur in the derivation of U.]

Wang and Teter[16] assert that ''although the formula falls into two regions with different forms, there is no discontinuity at the boundary. There is no physical significance for the boundary of the two regions.'' This perhaps needs closer attention. As Lloyd and Sholl[29] note, there is indeed a *mathematical* significance to the boundary between the two functional forms for $U(\mathbf{g}_1,\mathbf{g}_2)$, with a discontinuity of the derivative occurring along here, as well as where $g_i=2k_F$. This is reminiscent of the discontinuity that occurs in $\chi_0(g)$ at $2k_F$, although in $U(\mathbf{g}_1,\mathbf{g}_2)$ the limiting slope differs from each side of the discontinuity. This might be thought significant since the analogous discontinuity in $\chi_0(g)$ is often regarded as the origin of Friedel oscillations,[27] which certainly have physically significant consequences for effective potentials.[31] However, it has been demonstrated[32] that these oscillations are reproduced with a fit to $\chi_0(g)$ that does not contain the discontinuity, i.e., they are a consequence of the function's shape rather than of the discontinuity itself. For our purposes (see below), it is important that there is likewise *no* crucial physical role for the discontinuities in $U(\mathbf{g}_1,\mathbf{g}_2)$, because soon we will be obliged to adopt a simplified representation of this function in which it is not possible to incorporate discontinuities depending on $q_3^2-4\sin^2\theta=0$.

Following Wang and Teter,[16] but with greater generality, we construct a kinetic-energy functional of the form

$$T_{\alpha\beta}[\rho]=T_\alpha[\rho]+\int_\Omega\int_\Omega\int_\Omega\Delta\rho^{(\beta)}(\mathbf{r}_1)\Delta\rho^{(\beta)}(\mathbf{r}_2)\Delta\rho^{(\beta)}\times(\mathbf{r}_3)K_{\alpha\beta}(|\mathbf{r}_1-\mathbf{r}_2|,|\mathbf{r}_1-\mathbf{r}_3|)d\mathbf{r}_1d\mathbf{r}_2d\mathbf{r}_3. \quad (2.10)$$

(Wang and Teter looked at the particular case $T_{5/6\,5/9}$.) $K_{\alpha\beta}$ can be obtained by forming the Euler-Lagrange equation from Eq. (2.10),[12] converting this to reciprocal space, substituting in Eq. (2.4) and extracting the term that is quadratic in $V(g)$. The resulting expression is

$$K_{\alpha\beta}(g_1,g_2,g_3)=\frac{1}{\beta^3\Omega^2\rho_0^{3\beta-1}}\left\{\frac{k_F^2}{18}+\frac{k_F^2}{16}[g_1^2+g_2^2+g_3^2]-\tfrac{1}{3}\alpha^2(\alpha-1)\Omega\rho_0^{2\alpha-1}\times[K_\alpha(g_1)+K_\alpha(g_2)+K_\alpha(g_3)]+\frac{k_F^5}{27\pi^6}\frac{I(g_1,g_2,g_3)}{\chi_0(g_1)\chi_0(g_2)\chi_0(g_3)}\right\}. \quad (2.11)$$

The selection of β remains to be made. It could be treated as a fitting parameter, but the restriction to values that are in some sense ''natural'' is preferred, as was done with α. The simplest possibility is $\beta=1$, which will not contribute to the higher-than-quadratic response behavior of the electrons. Then there is Wang and Teter's choice of 5/9. In this case the quadratic response term contains the density in the same fashion as it appears in the Thomas-Fermi term, which is $\rho_{\mathbf{g}_1}^{(5/9)}\rho_{\mathbf{g}_2}^{(5/9)}\rho_{\mathbf{g}_3}^{(5/9)}\delta_{\mathbf{g}_1+\mathbf{g}_2+\mathbf{g}_3}$ when cast within a triple reciprocal-space sum. By the following argument (similar to that for the linear response case), it can be demonstrated that functionals with $\beta=5/9$ are superior in situations of low average density. Wang and Teter note that the von Weiszäcker functional accounts for the quadratic response behavior of the electrons at short wavelengths, which gives further confirmation that the von Weiszäcker functional is the correct form in the limit of rapid spatial variations for perturbations of any magnitude. This means that the $g_1^2+g_2^2+g_3^2$ term in $K_{\alpha\beta}$ is canceled by $\chi_0^{-1}(g_1)\chi_0^{-1}(g_2)\chi_0^{-1}(g_3)I(g_1,g_2,g_3)$ as $q_1,q_2,q_3\to\infty$. We have already seen the behavior of $K_\alpha(g_i)$ in this limit. On its appearance within $K_{\alpha\beta}$ it is dressed in a coefficient that leaves it with a $\rho_0^{-4/3}$ dependence irrespective of α. The same is true of the other term remaining in $K_{\alpha\beta}$, so that for low average densities the overall behavior of $T_{\alpha\beta}$ goes as $\rho_0^{5/3-3\beta}$, which is eliminated by taking $\beta=5/9$.

We have investigated an extended family of such functionals: T_{11}, $T_{5/6\,1}$, $T_{5/6\,5/9}$, and $T_{1/2\,5/9}$. The results will be

discussed below. The functional that Wang and Teter[16] tested in detail was different again, comprising $T_{5/6\ 5/9}$ plus an expression which built in the second-order gradient expansion term at low g. $T_{1/2\ 5/9}$ also has this property, up to second order in the density. As the next term in the gradient expansion is *fourth* order in the gradient of the density,[12] it is beyond the scope of these functionals, which only directly include the third order in density. Wang and Teter state that adding the gradient expansion brought some improvement over $T_{5/6\ 5/9}$ alone, but they did not specify the extent of this improvement. Their work involved energy minimization calculations; they did not perform molecular-dynamics with their functional.

B. Recovering linear scaling

As it stands, the amount of computation required for $T_{\alpha\beta}[\rho]$ scales as the square of the system size; even after taking advantage of the translational invariance of $K_{\alpha\beta}(\mathbf{r}_1-\mathbf{r}_2,\mathbf{r}_1-\mathbf{r}_3)$ there remains a double integral over the spatial coordinate to be performed. A functional with linear scaling may be salvaged from this by replacing $K_{\alpha\beta}(g_1,g_2,g_3)$, by a separable function, that is, a sum of terms having the form $f_a(g_1)f_b(g_2)f_c(g_3)$, which give a good fit to $K_{\alpha\beta}$, and then exploiting the convolution theorem. Wang and Teter[16] devised a separable fit for $K_{5/6\ 5/9}$, and as $K_{\alpha\beta}(g_1,g_2,g_3)-K_{5/6\ 5/9}(g_1,g_2,g_3)$ is already in separable form, the generalization to $K_{\alpha\beta}$ is straightforward:

$$K^{\rm fit}_{\alpha\beta}(g_1,g_2,g_3)=\frac{-k_F^2}{\beta^3\Omega^2\rho_0^{3\beta-1}}\{\Gamma(q_1,q_2,q_3)f_1(q_1)f_1(q_2)f_1(q_3)+f_2(q_1)f_2(q_2)f_2(q_3)[f_3(q_1)+f_3(q_2)+f_3(q_3)]$$
$$+f_4(q_2)f_4(q_3)f_5(q_1)+f_4(q_3)f_4(q_1)f_5(q_2)+f_4(q_1)f_4(q_2)f_5(q_3)+f_6(q_1)f_7(q_2)f_7(q_3)$$
$$+f_6(q_2)f_7(q_3)f_7(q_1)+f_6(q_3)f_7(q_1)f_7(q_2)+\Delta K_\alpha(g_1)+\Delta K_\alpha(g_2)+\Delta K_\alpha(g_3)\}, \tag{2.12}$$

where $q=g/k_F$, $\Delta K_\alpha(g)=\alpha^2\Omega\rho_0^{2\alpha-1}/18k_F^2(6\alpha-5)K_\alpha(g)$ [based on the difference between $K_\alpha(g)$ and $K_{5/6}(g)$], and where Wang and Teter's fitting functions Γ and $f_{1\to7}$ are given in the Appendix. $T_{\alpha\beta}[\rho]$ can then be expressed in terms of Fourier transforms (denoted $\mathscr{F}$, and $\mathscr{F}^{-1}$ for the inverse transform) between real and reciprocal space:

$$T_{\alpha\beta}[\rho]=T_\alpha[\rho]-\frac{k_F^2}{\beta^3\rho_0^{3\beta-1}}\int_\Omega\{-\tfrac{13}{540}F_1(\mathbf{r})^3-\tfrac{1}{40}F_2(\mathbf{r})F_3(\mathbf{r})^2$$
$$+\tfrac{1}{20}F_4(\mathbf{r})F_3(\mathbf{r})F_1(\mathbf{r})+3F_5(\mathbf{r})F_6(\mathbf{r})^2$$
$$+3F_7(\mathbf{r})F_8(\mathbf{r})^2+3F_9(\mathbf{r})F_{10}(\mathbf{r})^2$$
$$+3F_{11}(\mathbf{r})\{\Delta\rho^{(\beta)}(\mathbf{r})\}^2\}d\mathbf{r}, \tag{2.13}$$

where, if $\rho_{\mathbf{g}}^{(\beta)}=\mathscr{F}[\Delta\rho^{(\beta)}(\mathbf{r})]$, then $F_1(\mathbf{r})=\mathscr{F}^{-1}[\rho_{\mathbf{g}}^{(\beta)}f_1(g)]$, and the remaining auxiliary functions are given in the Appendix. With the aid of fast Fourier transformation, this expression can be calculated in a time proportional to $\Omega\log\Omega$. The calculation of the energy functional requires 12 Fourier transforms.

We have examined the agreement between $K_{\alpha\beta}$ and $K^{\rm fit}_{\alpha\beta}$ by looking at each function using computer programs for three-dimensional visualization. The results are excellent, in view of the complexity of the function, with relative errors of less than 1% almost everywhere. We have also compared third order energies obtained from the fitted function for certain input densities with those obtained from the exact expression. Here, agreement was better than 0.5% even when the input density was that for the ground state of a metallic liquid. These comparisons are discussed in more detail elsewhere.[33] They give us confidence that the errors introduced with the fitted kernel are insignificant.

To perform *ab initio* molecular dynamics and efficient energy minimizations, we also require $\delta(T_{\alpha\beta}-T_\alpha)/\delta\rho_{\mathbf{g}}$. With the help of the chain rule, this can be expressed as $\mathscr{F}\{\beta\rho^{\beta-1}(\mathbf{r})\mathscr{F}^{-1}[\delta(T_{\alpha\beta}-T_\alpha)/\delta\rho_{\mathbf{g}}^{(\beta)}]\}$. Functional differentiation gives

$$\frac{\delta(T_{\alpha\beta}-T_\alpha)}{\delta\rho_{\mathbf{g}}^{(\beta)}}=\frac{-k_F^2}{\beta^3\rho_0^{3\beta-1}}\left\{\frac{f_1(q)}{20}\left[-\tfrac{13}{9}G_1(\mathbf{g})-\frac{1}{q^2}G_2(\mathbf{g})-\frac{q^4}{2}G_3(\mathbf{g})+G_4(\mathbf{g})-\frac{1}{q^2}G_5(\mathbf{g})+q^2G_6(\mathbf{g})\right]\right.$$
$$+3f_2(q)[2G_7(\mathbf{g})+f_3(q)G_8(\mathbf{g})]+6f_4(q)G_9(\mathbf{g})+3f_5(q)G_{10}(\mathbf{g})+6f_7(q)G_{11}(\mathbf{g})$$
$$\left.+3f_6(q)G_{12}(\mathbf{g})+6G_{13}(\mathbf{g})+3\Delta K_\alpha(g)G_{14}(\mathbf{g})\right\}, \tag{2.14}$$

where $G_1(\mathbf{g})=\mathscr{F}[F_1(\mathbf{r})^2]$, and the remaining functions $G_{2\rightarrow 14}$ are specified in the Appendix. So, with an additional 16 Fourier transforms we acquire the electronic forces as well, and the calculation of these over all $\mathbf{g}$ scales almost linearly.

III. TOTAL-ENERGY RESULTS ON ALUMINUM

Since aluminum exposed the limitations of the linear response functionals,[2] this was where we began our evaluation of the new functionals. As with the earlier work, we have used the local pseudopotential of Goodwin *et al.*,[24] which has been found[23,24] to give a reasonable representation of aluminum in Kohn-Sham calculations. Furthermore, Robertson *et al.*[22] have produced a database of total energies for different aluminum structures using the Goodwin potential, so that this potential is an excellent test bed.

In our work, as in Ref. 2, an energy cutoff of around 380 eV in the plane-wave representation of the electrons was required to yield convergence of the energies in the calculations. The high cutoff, relative to that which might be used in a K-S calculation with the same pseudopotential, is because this is the cutoff on the *density* expansion (i.e., twice the normal wave-function cutoff). Also, working with a very-well-converged density simplifies the evaluation of the gradient of the density. One problem we found in dealing with those terms in the forces (2.14) which involve the transforms of products of real-space functions is the generation of spurious forces due to ''aliasing'' of the Fourier transforms.[34] This problem is eliminated by ''padding'' the transforms, i.e., by extending the range of the functions to be transformed from reciprocal to real space with zeroes to eliminate spurious Fourier components.

A. Energies of various crystal structures

We performed energy minimization calculations using the second-order response functionals, for five of the structures studied by Robertson *et al.*[22]—face-centered cubic (fcc), body-centered cubic (bcc), simple cubic (sc), a ''vacancy lattice'' (VL), which is an fcc lattice with one atom in the unit cube removed, and diamond (D)—with the nearest-neighbor distance being 2.85 Å in each case. Convergence of the steepest descent proved more difficult[33] for some of the crystal structures when $\alpha=5/6$ than for 1, and most difficult for 1/2, but this was simply overcome by taking a smaller steepest-descent step. It seems probable that this is associated with the symmetry of the effective response about the uniform density limit. T_{11} is more symmetrical than the functionals with fractional powers of the density fluctuations and may behave better under the conditioning. Table I shows the resulting energies per atom (in eV), as well as those of Ref. 22. Figure 1 collects $T_\alpha{}^2$ and $T_{\alpha\beta}$ results for $\alpha=1$, $\frac{5}{6}$, and $\frac{1}{2}$, respectively, each in comparison with the orbital-based calculations.

It can be seen that, in most cases, adding the quadratic response term substantially improves agreement with the orbital-based calculations. (In the few instances where this is not so, for instance the simple cubic energy when $\alpha=5/6$, the worsening is only slight.) For the orbital-based calculations, $E_{\rm VL}<E_{\rm sc}$. Using T_1 and $T_{5/6}$ the ordering is switched, but the introduction of the quadratic response term corrects this. Also in the orbital-based calculations, $E_{\rm VL}$ is closer to $E_{\rm bcc}$ than to $E_{\rm sc}$. Having $\beta=1$ fails to achieve this, but $\beta=5/9$ is successful. A good treatment of the vacancy lattice energy is of particular interest because it is related to the calculation of the experimentally observable vacancy formation energy, an issue we will address below. The best behaved of the quadratic response functionals appears from these calculations to be $T_{5/6\ 5/9}$.

TABLE I. The energies per atom, in electron volts, for various crystal structures calculated with different $T_{\alpha\beta}$ functionals are compared with the orbital-based results of Robertson *et al.* (Ref. 22), denoted K-S.

	T_{11}	$T_{5/6\ 1}$	$T_{5/6\ 5/9}$	$T_{1/2\ 5/9}$	K-S
fcc	-58.32	-58.33	-58.34	-58.34	-58.31
bcc	-58.25	-58.26	-58.25	-58.26	-58.24
VL	-58.01	-58.05	-58.16	-58.19	-58.10
sc	-57.98	-58.01	-58.04	-58.06	-57.91
D	-57.10	-57.27	-57.40	-57.47	-57.42

B. Properties of the fcc crystal

For the equilibrium crystal structure, which is the fcc lattice, we performed energy minimization calculations for a range of slightly different densities and fit a parabola to the resulting $E(\Omega)$. From this we could ascertain the equilibrium unit-cell length $a_{\rm lat}$ and the bulk modulus $B=\Omega(d^2E/d\Omega^2)|_{\Omega=a_{\rm lat}^3}$. This was done for T_{11}, $T_{5/6\ 1}$, and $T_{5/6\ 5/9}$, and the results are shown in Table II, together with values from experiment,[25,26] from the T_α calculations,[2] and from K-S calculations of Gillan.[23] The values for $a_{\rm lat}$ were in excellent agreement with the Kohn-Sham and experimental results, and were an improvement over those from the linear response functionals. The bulk modulus was unchanged for $\alpha=1$, but deteriorated slightly on addition of quadratic response when $\alpha=5/6$.

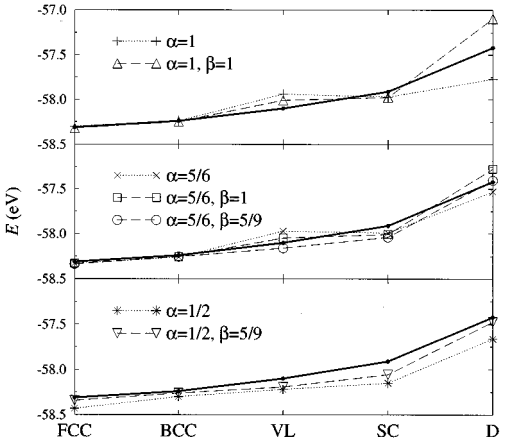

FIG. 1. Energies of various aluminum crystal structures, for T_α (dotted lines), $T_{\alpha\beta}$ (dashed lines), and orbital-based (thick lines) functionals.

TABLE II. Calculated physical properties of Al compared with experimental results. $a_{\rm lat}$: lattice parameter (Å). B: bulk modulus (Mbar). E_f^u: formation energy of the ideal vacancy (eV). E_f^r: formation energy of the relaxed vacancy (eV). K-S and experimental data from Refs. 23–26. For $T_{5/6\ 5/9}$ results are available on 32- and 108- (lower) atom cells.

	T_1	$T_{5/6}$	$T_{1/2}$	T_{11}	$T_{5/6\ 1}$	$T_{5/6\ 5/9}$	$T_{1/2\ 5/9}$	K-S	Expt.
$a_{\rm lat}$	4.059	4.038	3.964	4.038	4.033	4.027	4.023	4.022	4.043
B	0.70	0.72	0.69	0.70	0.69	0.67	0.66	0.79	0.74
E_f^u	1.63	1.38	0.21	1.14	1.02	0.40 0.37	0.26	0.64	
E_f^r				0.94	0.83	0.31 0.29		0.56	0.66

Gillan[23] suggested a useful way of exploring the contributions of different orders of response theory to the total energy. The ionic pseudopotential $V(\mathbf{g})$ is scaled by a constant C for all $\mathbf{g}$, and calculations of the total energy, $E(C)$, are made for various choices of C between 0 and 1. It is then possible to look at the perturbation behavior of the valence electron cloud for various orders of V. We can write

$$E(C)=E^{(0)}+CE^{(1)}+C^2E^{(2)}+C^3E^{(3)}+\cdots. \quad (3.1)$$

The energy of the same ionic arrangement but with a uniform electron cloud $E_{\rho_0}(C)=E^{(0)}+CE^{(1)}$, so that $\Pi(C)=[E(C)-E_{\rho_0}(C)/NC^2]=E^{(2)}+CE^{(3)}+\cdots$, and a plot of $\Pi(C)$ versus C will give a curve whose $C=0$ intercept will be determined by the linear response of the electrons to the applied potential, while the slope in the limit $C\to 0$ will be determined by the quadratic response, and so on.

Such an analysis has already been done by Gillan[23] with the Kohn-Sham functional and Smargiassi and Madden[2] using T_α, and a graph with their results together with those for the $T_{\alpha\beta}$ functionals is presented in Fig. 2. The calculations were performed at the experimental lattice parameter (Table II). It was found that great care was necessary to ensure that all the components of the energies were being calculated to sufficient accuracy, as for small C the differences being taken were of large, very similar numbers. Whereas of the linear response functionals, only $T_{5/6}$ lies along the Kohn-Sham curve, indicating that for this system it has captured the correct higher-order behavior as well as the built-in linear response behavior, the others start with the correct $C=0$ intercept (as they should, by construction) but then move away with the wrong slope. The quadratic response functionals all lie along the Kohn-Sham results; they have both linear and quadratic response behavior correctly built in, and they also seem to be describing the higher orders well in this case.

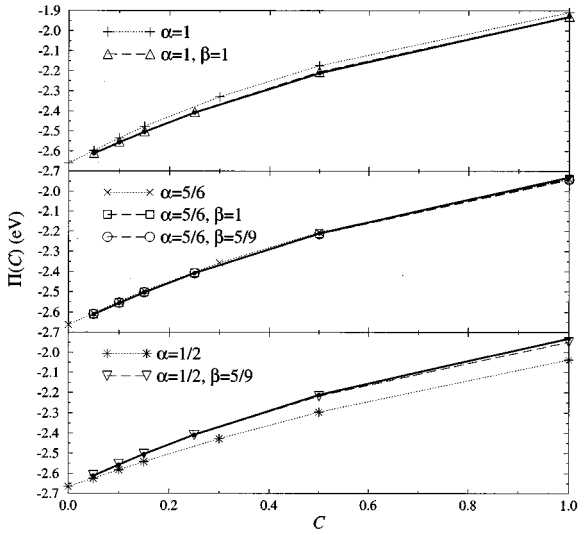

FIG. 2. Electronic energy per atom for the Al crystal vs scaling parameter C. K-S results are for a 27-atom cell [after Gillan (Ref. 23)].

C. Vacancy

A vacancy in an infinite fcc lattice can be approximated by a periodically replicated fcc lattice with one atom removed, provided that the simulation cell is large enough to make vacancy-vacancy interactions negligible. We calculate $E_{\rm vac}$, the energy of a cell having one less atom with the cell volume reduced so as to maintain constant ionic density. The (unrelaxed) vacancy formation energy is then

$$E_f^u=E_{\rm vac}-\frac{N-1}{N}E, \quad (3.2)$$

where E is the energy of the perfect crystal cell with N ions. As shown in Table II, for each α, the unrelaxed vacancy formation energy for a 32-atom fcc cell has improved on addition of the quadratic response correction, and moved towards the Kohn-Sham values, which are for a 27-atom fcc cell. For $T_{5/6\ 5/9}$ we achieve almost respectable agreement. E_f^u for the same functional applied to a 108-atom fcc cell only changes by 0.03 eV, showing that our results are not much affected by the presence of periodic images of the vacancy.

We can repeat the perturbation analysis, this time for the vacancy formation. Taking $E(C)$ as defined in Sec. III B, and $E_{\rm vac}(C)$ to be the corresponding energy for the vacancy system having one less atom with the cell volume reduced so as to maintain constant ionic density, we can calculate

$$E_f^u(C)=E_{\rm vac}(C)-\frac{N-1}{N}E(C). \quad (3.3)$$

In Fig. 3, we plot $\Pi_f^u=E_f^u(C)-E_f^u(\rho_0,C)/C^2$ against C. This elucidates the benefits of the quadratic response term.

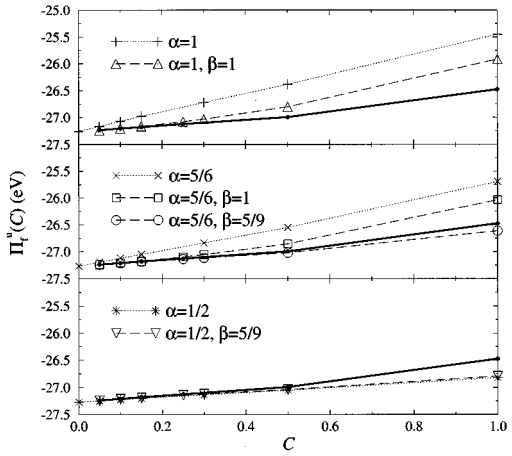

FIG. 3. Formation energy of the Al vacancy as a function of the pseudopotential scaling parameter C. A 32-atom cell was used, except for the K-S results,[23] which were obtained using a 27-atom cell.

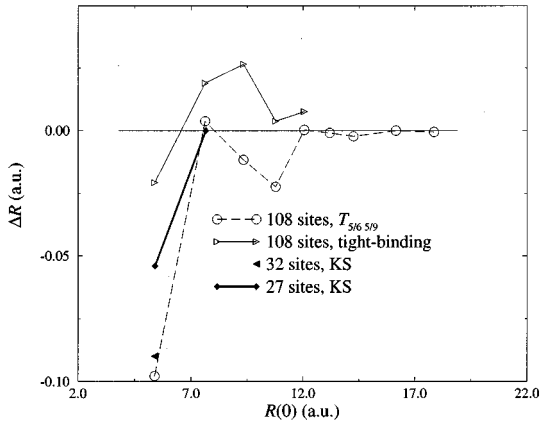

FIG. 4. The ionic relaxation away from the vacancy site versus initial distance from the site. The current results (open circles) are compared with those from several orbital-based calculations: open triangles, Ref. 21; filled triangles, Ref. 36; filled diamonds, Ref. 37.

Again, all the functionals exhibit the correct $C\rightarrow 0$ limit, but for this system the limiting slope as $C\rightarrow 0$ is incorrect for each of the linear response T_α functionals. This is clearly improved in all the $T_{\alpha\beta}$ functionals.

It is interesting to consider the influence of the quadratic response kernel at yet higher orders, by looking at the curvature moving away from $C=0$. For $\beta=1$ there should be no higher-order contributions from this term, and indeed the curves for T_α and $T_{\alpha 1}$ move in parallel once beyond the initial change in slope. With $\beta=5/9$ higher-order contributions are expected, and $T_{5/6\ 5/9}$ does curve differently from $T_{5/6}$. In this case, the contributions appear to be such as lead to an improvement in the vacancy formation energy. As seen in Sec. III B, there does seem to be a trend in that the functional forms that smoothly combine the linear/quadratic response with the Thomas-Fermi limiting form do best in approximating higher orders of response behavior.

For three of our functionals we found the vacancy relaxation energy E_r—the energy released when the ions are allowed to relax to their equilibrium positions using a steepest-descent algorithm. The relaxed vacancy formation energy is then

$$E_f^r=E_f^u-E_r\,. \tag{3.4}$$

The results are displayed in Table II. The lowering in energy in each case is comparable to that witnessed in the Kohn-Sham calculations. Although the inclusion of the second-order response terms has greatly improved the predicted vacancy properties, none of the functionals quite achieves the level of agreement with experiment found in the Kohn-Sham calculations.[23]

Figure 4 shows the change in the distance of the ions from the vacancy after relaxation from their perfect lattice sites. This is for the 108-1 atom system with the $T_{5/6\ 5/9}$ functional. As the distances of the lattice sites from the vacancy approach half the cell length, the amount of relaxation goes to zero, due to the balancing influence of periodic images of the vacancy. The oscillations in the relaxation are due to Friedel oscillations in the screened ion-ion potential. On the figure, the behavior of the present calculation is compared to some other *ab initio* results. Full Kohn-Sham calculations have been performed by Benedek *et al.*[36] (for a 32-atom system) and Mehl and Klein[37] (for 27), using different nonlocal pseudopotentials. These results agree well with ours for the near-neighbor displacements. The calculation of Caro *et al.*[21] is the only other calculation to use 108 sites. It employs an approximate Kohn-Sham–based scheme:[35] the valence electrons are treated as being tightly bound to the ions, with the orbitals centered on the ions and restricted in extent, and the assumption is made that the electron density only deviates linearly from the superposition of the atomic electron densities. Although they, too, see oscillations, the positioning and extent of these are rather different from ours.

IV. MOLECULAR DYNAMICS—CALCULATION OF PHONON FREQUENCIES

Car-Parrinello molecular-dynamics simulations were performed on a 32-atom periodic fcc lattice, at the experimental density and a temperature of 75 K. The computation time required per step was 6.7 s on a Silicon Graphics Indigo^2 (R8000) workstation. For T_{11}, a 108-atom lattice was also simulated. Each step took 23.3 s and so we have achieved nearly linear scaling of computational effort with system size. (This is spoiled only by the evaluation of the electron-ion interactions and the collection of the correlation functions, operations that scale as Ω^2.) A time step of 0.3 fs was used in both calculations—considerably larger than that normally used in K-S Car-Parrinello molecular dynamics. This is due to the ''conditioning'' of the algorithm that was applied exactly as described elsewhere,[1] even though a different density-functional is in use. The electronic degrees of freedom were conditioned to oscillate in the vicinity of 2600 ps^{-1}.[1] Unlike normal K-S *ab initio* MD simulations of metals, no recourse to thermostatting was required.[8,38]

Phonon frequencies were obtained from the spectra of the correlation functions of the longitudinal and transverse ion currents

$$C^L(\mathbf{k},t)=\left\langle\left(\sum_{j=1}^{N}-i\mathbf{k}\cdot\mathbf{v}^j(t)e^{-i\mathbf{k}\cdot\mathbf{r}^j(t)}\right)\left(\sum_{l=1}^{N}i\mathbf{k}\cdot\mathbf{v}^l(t)e^{i\mathbf{k}\cdot\mathbf{r}^l(t)}\right)\right\rangle, \tag{4.1}$$

$$C^T(\mathbf{k},t)=\left\langle\left(\sum_{j=1}^{N}-i\mathbf{k}\times\mathbf{v}^j(t)e^{-i\mathbf{k}\cdot\mathbf{r}^j(t)}\right)\left(\sum_{l=1}^{N}i\mathbf{k}\times\mathbf{v}^l(t)e^{i\mathbf{k}\cdot\mathbf{r}^l(t)}\right)\right\rangle, \tag{4.2}$$

where $\mathbf{r}^j$ and $\mathbf{v}^j$ are the position and velocity of ion j. The phonon dispersion curves are shown in Fig. 5. Kohn-Sham results are available for the zone center and boundary[23] for the same pseudopotential, and agreement with these is excellent for all of the quadratic response functionals. The results are substantially better than those for the linear response functionals, which were all too low by about the same amount, as represented on the figure by the T_1 curves. All of the simulation results fall below the experimental curves;[39] this failing can be attributed to inadequacies in the Goodwin pseudopotential, which they all use. The T_{11} simulation on the 108-atom lattice allowed some of the intervening points on its dispersion curve to be filled in.

V. DISCUSSION

The orbital-free functionals incorporating the correct linear response that have hitherto been used for *ab initio* molecular dynamics have permitted an electronic calculation that scales with Ω, but have not achieved the accuracy of the more usual Kohn-Sham methods. Following the work of Wang and Teter, we have developed a family of functionals that include the correct quadratic response, and have demonstrated in the case of aluminium that, while retaining the desired scaling characteristics, they give results much closer to, and in some instances matching, those from Kohn-Sham calculations. We have also shown that these functionals can be used successfully for molecular dynamics.

Theoretical questions remain. How best to select α and β, and hence the specific functional form, has not been resolved. It seems that $T_{5/6\,5/9}$, the choice Wang and Teter made in the first place, tends to give better results. Is there a fundamental reason for the superiority of the Thomas-Fermi–like expressions obtained with $\alpha=5/6$ and $\beta=5/9$? Are there ways of including the second-order gradient expansion other than choosing $\alpha=1/2$, which gives poorer results than 5/6, or using Wang's and Teter's unsatisfyingly *ad hoc* method, which they claim leads to improved results?

The present usefulness of the orbital-free functionals is restricted by the lack of good local pseudopotentials to represent the ions. Much of the effort in developing pseudopotentials has gone into nonlocal pseudopotentials that depend on *orbital* angular momentum, for which we have no representation in the present orbital-free technique. In the short term, progress can be made by investigating new local pseudopotentials, but the long-term usefulness of what is otherwise a very promising approach can only be assured by finding ways to include aspects of nonlocality into the orbital-free formalism. Attempts to do this are being made, for instance by Wang[40] and Kanhere and co-workers.[41]

For those atoms (Na, Al, Ge, . . .) for which reasonable local pseudopotentials are available, we are now in a position to be able to perform large-scale simulations of systems of hundreds and even (with the help of parallelization) thousands of atoms over periods of many tens of picoseconds, to an accuracy approaching that of standard *ab initio* simulations. Various applications are underway.

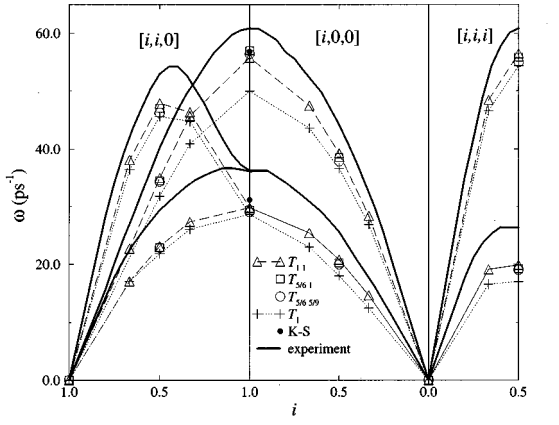

FIG. 5. Phonon dispersion curves for Al at 75 K, as calculated using orbital-free *ab initio* molecular dynamics (crosses). Experimental data (lines) from Ref. 39; K-S values (squares) from Ref. 24.

ACKNOWLEDGMENTS

Michael Foley is grateful to the Association of Commonwealth Universities for their financial assistance. This work was sponsored by EPSRC (UK) through Grant No. GR/H10276.

APPENDIX A

In this appendix we collect a number of the functions used in the separable representation of the second-order integral kernel. A Fourier transform from real to reciprocal space is denoted $\mathscr{F}$ and its inverse $\mathscr{F}^{-1}$ and $q=g/k_F$.

The following functions were introduced by Wang and Teter in their separable representation [Eq. (2.12)]:

$$\Gamma(q_1,q_2,q_3)=-\frac{13}{540}-\frac{1}{120}\left\{\frac{q_1^4}{q_2^2q_3^2}+\frac{q_2^4}{q_3^2q_1^2}+\frac{q_3^4}{q_1^2q_2^2}-\frac{q_2^2}{q_1^2}-\frac{q_1^2}{q_2^2}-\frac{q_2^2}{q_3^2}-\frac{q_3^2}{q_2^2}-\frac{q_1^2}{q_3^2}-\frac{q_3^2}{q_1^2}\right\}, \tag{A1}$$

$$f_1(q)$$

$$=\begin{cases} \dfrac{0.4q^2}{1+\left(\dfrac{q}{2.33}\right)^{10}}, & q\leqslant 1.95 \\ \dfrac{0.06}{(q-1.835)^{0.75}}+0.05(k-1.8)e^{-2.5(q-2)}+1, & q\geqslant 1.95, \end{cases} \tag{A2}$$

$$f_2(q)=\frac{1}{2}+\frac{q^2-4}{8q}\ln\left|\frac{2-q}{2+q}\right|, \tag{A3}$$

$$f_3(q)=\begin{cases} \dfrac{-\dfrac{1}{81}q^2-0.002q^4}{1+\left(\dfrac{q}{1.955}\right)^{28}}, & q\leqslant 1.84 \\ -0.055e^{-4.2(q-1.84)}, & q\geqslant 1.84, \end{cases} \tag{A4}$$

$$f_4(q)=\begin{cases} 1, & q\leqslant 2 \\ e^{-3(q-2)}, & q\geqslant 2, \end{cases} \tag{A5}$$

$$f_5(q)=\begin{cases} 0.02e^{-30(q-2.15)^2}, & q\leqslant 2.15 \\ 0.02e^{-1.8(q-2.15)^2}, & q\geqslant 2.15, \end{cases} \tag{A6}$$

$$f_6(q)=-0.017e^{-(q-3)^2}, \tag{A7}$$

and

$$f_7(q)=\begin{cases} 0, & q\leqslant 0.7 \\ \dfrac{q-1.95}{1.25}+1, & 0.7\leqslant q\leqslant 1.95 \\ e^{-2(q-1.95)}, & q\geqslant 1.95. \end{cases} \tag{A8}$$

The following definitions are exploited in Eq. (2.13):

$$F_1(\mathbf{r})=\mathscr{F}^{-1}[\rho_{\mathbf{g}}^{(\beta)}f_1(q)], \quad F_2(\mathbf{r})=\mathscr{F}^{-1}[\rho_{\mathbf{g}}^{(\beta)}f_1(q)q^4],$$

$$F_3(\mathbf{r})=\mathscr{F}^{-1}[\rho_{\mathbf{g}}^{(\beta)}f_1(q)/q^2], \quad F_4(\mathbf{r})=\mathscr{F}^{-1}[\rho_{\mathbf{g}}^{(\beta)}f_1(q)q^2],$$

$$F_5(\mathbf{r})=\mathscr{F}^{-1}[\rho_{\mathbf{g}}^{(\beta)}f_2(q)f_3(q)], \quad F_6(\mathbf{r})=\mathscr{F}^{-1}[\rho_{\mathbf{g}}^{(\beta)}f_2(q)],$$

$$F_7(\mathbf{r})=\mathscr{F}^{-1}[\rho_{\mathbf{g}}^{(\beta)}f_5(q)], \quad F_8(\mathbf{r})=\mathscr{F}^{-1}[\rho_{\mathbf{g}}^{(\beta)}f_4(q)],$$

$$F_9(\mathbf{r})=\mathscr{F}^{-1}[\rho_{\mathbf{g}}^{(\beta)}f_6(q)], \quad F_{10}(\mathbf{r})=\mathscr{F}^{-1}[\rho_{\mathbf{g}}^{(\beta)}f_7(q)],$$

and

$$F_{11}(\mathbf{r})=\mathscr{F}^{-1}[\rho_{\mathbf{g}}^{(\beta)}K_{\alpha}^{\Delta}(g)].$$

The following definitions are exploited in Eq. (2.14):

$$G_1(\mathbf{g})=\mathscr{F}[F_1(\mathbf{r})^2], \quad G_2(\mathbf{g})=\mathscr{F}[F_2(\mathbf{r})F_3(\mathbf{r})],$$

$$G_3(\mathbf{g})=\mathscr{F}[F_3(\mathbf{r})^2], \quad G_4(\mathbf{g})=\mathscr{F}[F_4(\mathbf{r})F_3(\mathbf{r})],$$

$$G_5(\mathbf{g})=\mathscr{F}[F_4(\mathbf{r})F_1(\mathbf{r})], \quad G_6(\mathbf{g})=\mathscr{F}[F_3(\mathbf{r})F_1(\mathbf{r})],$$

$$G_7(\mathbf{g})=\mathscr{F}[F_5(\mathbf{r})F_6(\mathbf{r})], \quad G_8(\mathbf{g})=\mathscr{F}[F_6(\mathbf{r})^2],$$

$$G_9(\mathbf{g})=\mathscr{F}[F_7(\mathbf{r})F_8(\mathbf{r})], \quad G_{10}(\mathbf{g})=\mathscr{F}[F_8(\mathbf{r})^2],$$

$$G_{11}(\mathbf{g})=\mathscr{F}[F_9(\mathbf{r})F_{10}(\mathbf{r})], \quad G_{12}(\mathbf{g})=\mathscr{F}[F_{10}(\mathbf{r})^2],$$

$$G_{13}(\mathbf{g})=\mathscr{F}[F_{11}(\mathbf{r})\Delta\rho^{\beta}(\mathbf{r})],$$

and

$$G_{14}(\mathbf{g})=\mathscr{F}[\{\Delta\rho^{\beta}(\mathbf{r})\}^2].$$

[1] M. Pearson, E. Smargiassi, and P. A. Madden, J. Phys. Condens. Matter **5**, 3321 (1993).
[2] E. Smargiassi and P. A. Madden, Phys. Rev. B **49**, 5220 (1994).
[3] R. Car and M. Parrinello, Phys. Rev. Lett. **55**, 2471 (1985).
[4] G. Galli and A. Pasquarello, in *Computer Simulations in Chemical Physics*, edited by M. P. Allen and D. J. Tildesley (Kluwer, Dordrecht, 1993).
[5] D. K. Remler and P. A. Madden, Mol. Phys. **70**, 921 (1990).
[6] W. Kohn and L. J. Sham, Phys. Rev. **140**, A1133 (1965).
[7] G. Pastore, E. Smargiassi, and F. Buda, Phys. Rev. A **44**, 6334 (1991).
[8] P. E. Blöchl and M. Parrinello, Phys. Rev. B **45**, 9413 (1992).
[9] M. Foley, E. Smargiassi, and P. A. Madden, J. Phys. Condens. Matter **6**, 5231 (1993).
[10] E. Smargiassi and P. A. Madden, Phys. Rev. B **51**, 117 (1995).
[11] E. Smargiassi and P. A. Madden, Phys. Rev. B **51**, 129 (1995).
[12] R. G. Parr and W. Yang, *Density Functional Theory of Atoms and Molecules* (Oxford University Press, Oxford, 1989).
[13] R. M. Dreizler and E. K. U. Gross, *Density Functional Theory* (Springer-Verlag, Berlin, 1990).
[14] C. F. von Weizsäcker, Z. Phys. **96**, 431 (1935).
[15] F. Perrot, J. Phys. Condens. Matter **6**, 431 (1994).
[16] L.-W. Wang and M. P. Teter, Phys. Rev. B **45**, 13 197 (1992).
[17] J. Hafner, *From Hamiltonians to Phase Diagrams* (Springer-Verlag, Berlin, 1987).
[18] P. Hohenberg and W. Kohn, Phys. Rev. **136**, B864 (1964).
[19] A. Alavi, J. Kohanoff, M. Parrinello and D. Frenkel, Phys. Rev. Lett. **73**, 2599 (1994).
[20] W. C. Topp and J. J. Hopfield, Phys. Rev. B **7**, 1295 (1973).
[21] A. Caro, D. A. Drabold, and O. F. Sankey, Phys. Rev. B **49**, 6647 (1994).
[22] I. J. Robertson, V. Heine, and M. C. Payne, Phys. Rev. Lett. **70**, 1944 (1993).
[23] M. J. Gillan, J. Phys. Condens. Matter **1**, 689 (1989).
[24] L. Goodwin, R. J. Needs, and V. Heine, J. Phys. Condens. Matter **2**, 351 (1990).
[25] G. Simmons and H. Wang, *Single Crystal Elastic Constants and Calculated Aggregate Properties: A Handbook* (MIT Press, Cambridge, MA, 1971).
[26] K. A. Gschneidner, *Solid State Physics* (Academic Press, New York, 1964), Vol. 16, p. 275.
[27] N. W. Ashcroft and N. D. Mermin, *Solid State Physics* (Holt-

Saunders, New York, 1976); W. A. Harrison, *Solid State Theory* (McGraw-Hill, New York, 1970).
[28] R. O. Jones and O. Gunnarson, Rev. Mod. Phys. **61**, 689 (1989).
[29] P. Lloyd and C. A. Sholl, J. Phys. C **1**, 1620 (1968).
[30] J. Hammerberg and N. W. Ashcroft, Phys. Rev. B **9**, 409 (1974).
[31] J. Hafner and V. Heine, J. Phys. F **13**, 2479 (1983); **16**, 1429 (1986).
[32] D. G. Pettifor and M. A. Ward, Solid State Commun. **49**, 291 (1984).
[33] M. Foley, Ph.D. thesis, Oxford University, 1995.
[34] W. H. Press, B. P. Flannery, S. A. Teukolsky, and W. T. Vetterling, *Numerical Recipes* (Cambridge University Press, Cambridge, 1989).
[35] O. F. Sankey and D. J. Niklewski, Phys. Rev. B **40**, 3979 (1989).
[36] R. Benedek, L. H. Yang, C. Woodward, and B. I. Min, Phys. Rev. B **45**, 2607 (1992).
[37] M. J. Mehl and B. M. Klein, Physica B **172**, 211 (1991).
[38] E. S. Fois, J. I. Penman, and P. A. Madden, J. Chem. Phys. **98**, 6361 (1993).
[39] *Magnetic Properties of Metals. Actinide Elements and their Compounds with Other Elements*, edited by Landolt-Börnstein, New Series, Group III, Vol. 19, Pt. f (Springer-Verlag, Berlin, 1991).
[40] L.-W. Wang (private communication) has demonstrated a representation of nonlocality in the orbital-free framework.
[41] V. Shah, D. Nehete, and D. G. Kanhere, J. Phys. Condens. Matter **6**, 10 773 (1994).